Bit-Loaded PAPR Reduction for High-Data-Rate Through-Metal Control Network Applications

Magdalena Bielinski, *Student Member, IEEE*, Guillermo Sosa, *Member, IEEE*, Kevin Wanuga, *Student Member, IEEE*, Richard Primerano, *Member, IEEE*, Moshe Kam, *Fellow, IEEE*, and Kapil R. Dandekar, *Senior Member, IEEE*

***Abstract*—Data transmission through metallic structures is commonly required in industrial control applications. In a number of these applications, mechanically penetrating the structure to pass cables and establish a wired communication link is either impossible or undesirable. Examples of such structures include metal bulkheads, pressure vessels, or pipelines. Ultrasonic signaling has been proposed as a solution for through-metal data transfer without penetrating the structure. The reverberant nature of the through-metal channel, however, can lead to significant intersymbol interference, limiting the data rate achievable by conventional single-carrier communication techniques. In this paper, we describe a through-metal communication technique that exploits the slow-varying nature of the ultrasonic channel to implement an orthogonal-frequency-division-multiplexing-based rate-adaptive peak-to-average power ratio (PAPR) reduction algorithm. Measurements of the proposed adaptive algorithm have demonstrated transmitted throughput rates of up to 14 Mbps while reducing PAPR by up to 3 dB and maintaining a bit error rate of 10^{-5} at average transmit powers of roughly 6 dBm. This enhancement provides the required throughput and error rate to support high-rate network applications in otherwise data-limited environments.**

***Index Terms*—Acoustic data transmission, adaptive modulation, orthogonal frequency-division multiplexing (OFDM), peak-to-average power ratio (PAPR) reduction.**

I. Introduction

INDUSTRIAL control network applications often necessitate the use of sensor data for system monitoring and maintenance, making reliable and efficient data and power transfer for industrial sensor networks a growing research area [1]–[9]. However, many of these control network applications require that data transfer be performed through metallic barriers. Passing cables through the impeding metal structure is often not possible or is highly undesirable. Ultrasonic signaling has been explored as an alternative method to through-metal communication that does not require the mechanical penetration of the obstructing metallic barrier [10]–[13].

Manuscript received February 6, 2013; revised May 7, 2013; accepted June 18, 2013. Date of publication July 3, 2013; date of current version October 18, 2013. This work was supported in part by the Office of Naval Research under Project N00014-11-1-0327: Below-Deck Electromagnetic Environment Characterization for RF Wireless Network Operation.

M. Bielinski is with the Department of Electrical and Computer Engineering, Drexel University, Philadelphia, PA 19104 USA (e-mail: mmb82@drexel.edu).

G. Sosa, K. Wanuga, R. Primerano, M. Kam, and K. R. Dandekar are with Drexel University, Philadelphia, PA 19104 USA.

Color versions of one or more of the figures in this paper are available online at http://ieeexplore.ieee.org.

Digital Object Identifier 10.1109/TIE.2013.2272283

The ultrasonic through-metal communication link exhibits severe echoing due to acoustic impedance mismatch at the junction between the transducer and the metallic barrier [14]. These echoes produce a large delay spread [15] that severely limits the coherence bandwidth of the channel. When using single-carrier communication techniques in this environment, complex equalizers are needed to mitigate the frequency selectivity in the ultrasonic channel. Physical layers employing this technique are limited, in practice, to maximum throughput rates of roughly 5 Mbps [14]–[17]. As a result, the ultrasonic through-metal link is a bottleneck to network throughput.

Similar to work in subsea acoustic communication, previous work has demonstrated that multicarrier or orthogonal frequency-division multiplexing (OFDM)-based systems are capable of achieving high data rate communication through metal walls [18]–[24]. OFDM is a modulation technique used to mitigate frequency selectivity in wideband channels by transmitting parallel narrow band data streams orthogonally. To further increase spectral efficiency in an OFDM-based framework, we add a subcarrier-based rate adaptive modulation algorithm known as adaptive bit loading (ABL), which strives to maximize throughput while constraining the probability of symbol estimation error.

One of the main drawbacks of OFDM is its generation of high peak-to-average power ratios (PAPRs) which becomes more significant as the number of OFDM subcarriers increases. The coherent addition of the parallel OFDM data streams results in power fluctuations that can be much higher than the average power of the OFDM message. In radio systems, large peaks in the transmitted signal can cause nonlinear modulation distortion, out-of-band radiation, and reduced transmission range. Similarly, high PAPR in the ultrasonic channel results in the inefficient use of system hardware due to the fact that the transmitted message is scaled to fit within the linear operating regions of the system's transmitter and receiver signal chains. This scaling limits the average power of the OFDM messages.

Extensive research has been devoted to PAPR reduction [25]–[28], including the OFDM symbol rotation and inversion algorithm provided by Tan and Bar-Ness [29]. We modify this rotation and inversion technique and apply it to the ultrasonic environment, where the transmitter may suffer high PAPR due to the large number of OFDM subcarriers used [19]–[24].

Reducing PAPR allows for more efficient use of the digital to analog and analog to digital converter dynamic range and results in higher average transmit power [30]. It stands to reason that improving the link quality by reducing PAPR

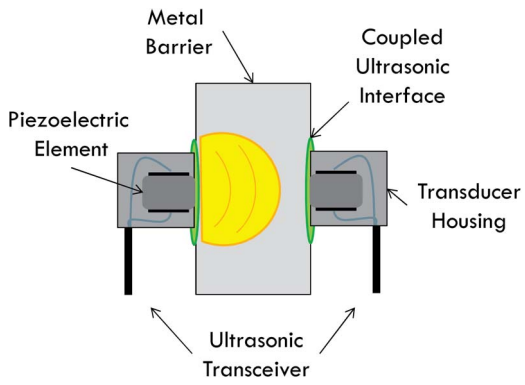

Fig. 1. Through-metal channel model.

will further improve the effectiveness of ABL since ABL approaches attempt to maximize throughput for a given link quality. Thus, extending the work performed in [18]–[21] to address PAPR, the contribution of this paper is the demonstration of this synergistic relationship between reduced PAPR and ABL in the ultrasonic through-metal channel for the same peak transmit power [30]. Furthermore, the slow-varying nature of this particular channel easily allows for the maintenance of the channel state information (CSI) required for rate adaptation, making the algorithm computationally tractable. Unlike in conventional wireless links, this CSI remains accurate over a long duration of time and therefore enables adaptation to channel conditions with limited overhead. The performance measurements of the proposed adaptive algorithm have demonstrated increased transmitted throughput rates while maintaining low BERs at average transmit powers near 6 dBm and reducing PAPR. This performance constitutes a significant data rate improvement over conventional through-metal communication techniques while meeting acceptable quality-of-service requirements.

II. Ultrasonic Through-Metal Channel

The ultrasonic through-metal channel is composed of the ultrasonic transducers and the metal barrier dividing them (see Fig. 1). The transmitting transducer generates acoustic waves driven by an electric voltage, and the receiving transducer converts this acoustic energy back into electric current.

Primerano *et al.* [15] experimentally demonstrated that the ultrasonic system shown in Fig. 1 is approximately linear with respect to an ensemble of rectangular pulse tests. Thus, we can model the system as having a transient response consisting of a primary resonant pulse and a series of delayed echoes. The echoing is caused by impedance mismatch, diffraction, and transceiver misalignment. Furthermore, this echoing is responsible for intersymbol interference (ISI) when using high-rate single-carrier modulation techniques [15].

To demonstrate the severity of echoing within the ultrasonic through-metal channel, an experimentally measured frequency sweep of the channel magnitude response for 0.25-in-thick mild steel is shown in Fig. 2. Impedance mismatch at the junction between the transducer and bulkhead causes reflections at the barrier. The reflection coefficient at this transducer–bulkhead

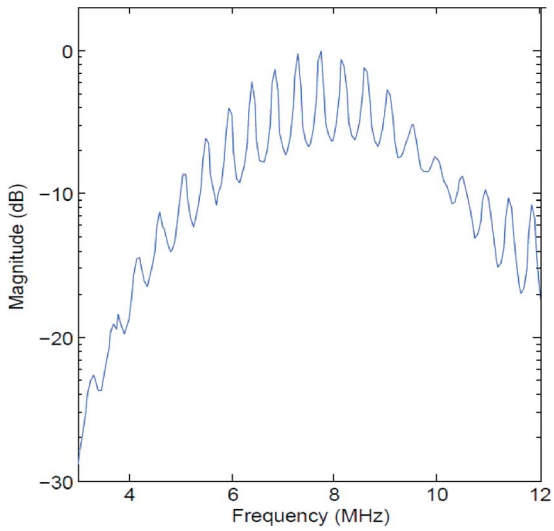

Fig. 2. Through-metal channel frequency response.

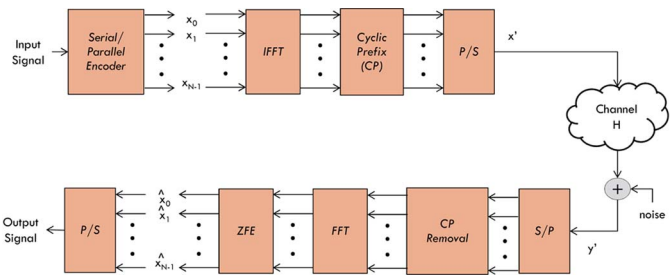

Fig. 3. Simplified OFDM block diagram.

junction is approximately -0.48 [15]. As seen in Fig. 2, deep nulls and high peaks occur within the magnitude response (i.e., it is highly frequency selective). The nulls are related to the acoustic echoing in the channel, where the spacing between nulls is equal to the reciprocal of the round-trip echo period of the channel. The physical thickness of the wall and the speed of sound in the metal determine this round-trip echo period.

The frequency selectivity observed in the acoustic channel of Fig. 2 makes high-speed communication a challenge when using single-carrier modulation techniques. Additionally, the long coherence time of the channel makes it an ideal environment for adaptive algorithms. In the following sections, the authors describe an OFDM-based adaptive algorithm designed to counteract the echo-induced channel interference without excessive overhead.

III. OFDM

The OFDM system depicted in Fig. 3 employs an $N = 512$ subcarrier OFDM frame. The OFDM message is limited to a bandwidth of 5 MHz due to the resonant bandwidth of the ultrasonic transducers. The OFDM subcarriers are spaced by approximately 10 kHz of bandwidth to ensure that a flat fading channel may be assumed for each subcarrier.

Direct up/down conversion is performed at the front end to exploit the in-phase and quadrature components of the carrier

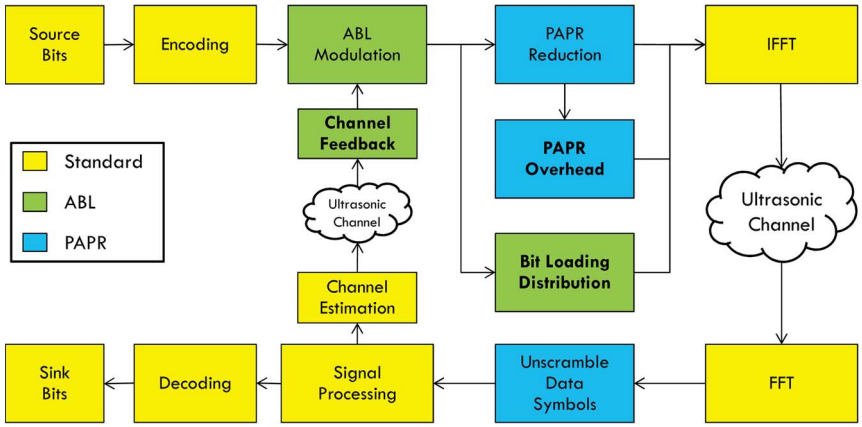

Fig. 4. Ultrasonic adaptive OFDM algorithm.

and allow for adaptive multilevel quadrature amplitude modulation (QAM). The transmitted baseband signal is composed of 512 orthogonal subcarriers, 496 of which carry data symbols. Non-data-carrying subcarriers include six pilot tones for correcting clock drift and residual carrier frequency offset and ten carriers reserved as a guard band to avoid interfering with energy from the carrier centered at 8.3 MHz. The physical layer implementation maps bits to symbols using M-QAM modulation, where $M = 2^i$, $i = \{1, 2, 4, 6, 8, 10\}$. The symbols are transmitted at a rate of 7.81 Ksymbols/s over the effective 5-MHz bandwidth.

The addition of a cyclic prefix to the OFDM frame is used to limit ISI from consecutive OFDM words. Assuming that each OFDM subcarrier is flat fading, the received signal of the kth subcarrier in Fig. 3 can be expressed as

$$y_k = \sqrt{e_k} h_k x_k + n_k \quad k = 1, 2, \ldots, N \tag{1}$$

where e_k is the power associated with the kth subcarrier, h_k and x_k are the kth subcarrier channel response and transmitted symbol, respectively, and n_k is the additive white Gaussian noise (AWGN) of the kth subcarrier. Noise is assumed to have zero mean and unit variance, and the time index has been removed for simplicity.

The receiver independently estimates h_k on each subcarrier from the sample mean of two training symbols as

$$\hat{h}_k = \frac{y_k}{x_k} = h_{tr_k} + \frac{n_{tr_k}}{\sqrt{e_k} x_{tr_k}}. \tag{2}$$

In (2), h_{tr_k} is the training channel, x_{tr_k} is the kth known training symbol, and n_{tr_k} is the kth subcarrier AWGN noise. The received OFDM symbols are corrected through zero-force equalization as shown in

$$\hat{x}_k = \frac{y_k}{\hat{h}_k} = \frac{\sqrt{e_k} h_k x_k}{\hat{h}_k} + \frac{n_{tr_k}}{\hat{h}_k}. \tag{3}$$

IV. Adaptive OFDM Communication Algorithm

A block diagram of the adaptive OFDM-based ultrasonic through-metal communication algorithm is provided in Fig. 4. Source data bits are encoded and modulated at the transmitter in accordance with the bit distribution calculated by the ABL algorithm [19]–[21] described in Section IV-A.

The rate adaptive algorithm relies on the assumption that the transmission channel remains stationary over a minimum duration of three packets. This limitation is due to the fact that an initial nonadaptive transmission must be performed to acquire the CSI at the receiver. For the ABL algorithm implemented here, this CSI is a size N array of error vector magnitudes (EVMs) calculated in (4) for each of the $k = 1, 2, \ldots, N$ subcarriers, where $\mathbb{E}\{\cdot\}$ is the expectation operator

$$EVM_k = \mathbb{E}\left\{|x_k - \hat{x}_k|^2\right\}. \tag{4}$$

It is assumed that the CSI is accessible to the transmitter in order to determine the optimal bit loading distribution. This optimal distribution is also conveyed from the transmitter to the receiver for proper decoding. While the channel must be stationary for a minimum of three packet transmissions, the ultrasonic channel fades very slowly in practice. This slow fading reduces the need for excessive channel training and limits the channel resources dedicated to training overhead.

After modulation, the PAPR is reduced through the symbol rotation and inversion algorithm by Tan and Bar-Ness [29] which finds the minimal PAPR symbol sequence upon symbol permutation in the frequency domain. Information regarding the number of rotations and inversions necessary to achieve the minimum PAPR sequence is stored and sent to the receiver, as shown in the "PAPR Overhead" block in Fig. 4. This information is used to recover the original data sequence prior to demodulation at the receiver.

Prior to transmission, the overhead information is appended to the data stream along with the preamble and header to construct the final OFDM packet. Note that, irrespective of the ABL data rates used on the data stream, all appended information is transmitted at a low data rate to ensure reliable decoding at the receiver. The data packet is converted to the time domain via an inverse fast Fourier transform (FFT). Upon reception, the data are converted back to the frequency domain via FFT, unscrambled using the PAPR overhead, equalized, demodulated, and decoded at the receiver. Additional details of the ABL and PAPR reduction techniques used in the proposed algorithm are described in the following sections.

A. ABL

A rate ABL algorithm given by Chow *et al.* [31] attempts to maximize the number of bits per OFDM symbol under a fixed energy and BER constraint. This algorithm is based on the signal-to-noise ratio (SNR) "gap," which provides an estimate of the additional power necessary for transmission using discrete constellations when compared to capacity-achieving Gaussian codebooks [32]. The gap concept relates the receiver SNR to a desired symbol error rate under the assumption of equally probable messages. The ultrasonic OFDM bit loading algorithm implemented here considers the relationship between the received SNR and the bit error probability of Gray-coded square M-QAM modulation through the use of the EVM of the training transmission [18]–[21].

The postprocessing SNR (PPSNR) for each individual subcarrier can be estimated by (5). Functions for the minimum PPSNR required to achieve a given probability of error in the range of 10^{-4}–10^{-6} using even M-QAM modulation orders were formulated to generate an offline lookup table. The algorithm performs modulation order decisions by comparing the measured estimates of the subcarrier-based PPSNR values to those in the lookup table such that the optimal distribution of bits among the subcarriers is allocated. If the SNR for the kth subcarrier is less than that required for 4-QAM, binary phase-shift keying (BPSK) is selected as the default modulation order

$$PPSNR_k = \frac{\mathbb{E}\left\{|x_k|^2\right\}}{EVM_k}. \tag{5}$$

Additional bit loading algorithms created by Campello [33] compute energy-tight bit distributions. This concept of tightening energy further optimizes ABL so that no other bit distribution can be calculated across all subcarriers such that an equivalent number of bits can be loaded with less average energy within the individual symbols. To ensure that the subcarriers remain energy tight, power scaling of the individual subcarriers is performed. Therefore, two variations of ABL have been developed for use in the proposed algorithm. The power-scaled rate adaptive (PSRA) variation is similar to those energy-tight algorithms developed by Campello [33], while the non-PSRA (NPSRA) algorithm does not scale power. Note that the NPSRA algorithm is suboptimal because it does not make efficient use of subcarrier symbol energy. Rather, the NPSRA variation assumes average unit power across all subcarriers.

B. PAPR Reduction

In the ultrasonic hardware used in this paper, high PAPR reduces the effective transmit power due to the inefficient use of the dynamic range of the transmit amplifier. To take full advantage of the hardware components in the ultrasonic implementation, a symbol rotation and inversion algorithm proposed by Tan and Bar-Ness [29] was adapted to the ultrasonic environment (which, with 512 subcarriers, has an increased sensitivity to PAPR [34]). Tan and Bar-Ness provide both optimal and suboptimal implementations of their algorithm. The algorithm implemented in this paper uses the suboptimal approach which has been shown to significantly reduce PAPR with the benefit of reduced complexity in comparison to the optimal approach.

1) Optimal Combined Symbol Rotation Algorithm: The *optimal combined symbol rotation* and *inversion* (O-CSRI) algorithm considers a set of N complex symbols, X_i, in an N subcarrier OFDM communication system, where pilot symbols are not permuted [29]. The sequence of symbols is divided into M blocks, each with (N/M) elements, where the ratio is an integer. The ith block can then be defined as

$$B_i = [X_{i1}, X_{i2}, \ldots, X_{i\frac{N}{M}}]. \tag{6}$$

Within each of these M blocks, the (N/M) symbols are rotated to generate a maximum of (N/M) blocks, $\tilde{B}_i^{(j)}$, where $j = 1, 2, \ldots, (N/M)$. To avoid having the same symbols occur in one OFDM block, another set of (N/M) blocks is also created by inverting the first (N/M) blocks such that

$$\underline{\tilde{B}_i}^{(j)} = -\tilde{B}_i^{(j)}.$$

Thus, an N-length OFDM sequence divided into M blocks will have a maximum of $(2N/M)^M$ unique sequence combinations. The symbol sequence with the smallest PAPR is selected for transmission, along with overhead regarding the number of rotations and inversions required to achieve this minimal PAPR. Overhead is necessary to recover the original OFDM sequence at the receiver and requires $M \log_2(2N/M)$ bits.

2) Successive Suboptimal Combined Symbol Rotation and Inversion Algorithm: The suboptimal approach to PAPR reduction discussed by Tan and Bar-Ness [29] is named the *successive suboptimal combine symbol rotation* and *inversion* (SS-CSRI) algorithm. In contrast to the O-CSRI implementation, the minimal PAPR is found successively—the random permutations are performed within each individual block (while keeping the other blocks the same) rather than performing permutations across all blocks. Therefore, the N complex symbols are first divided into blocks of (N/M) elements, as was done in the optimal approach. Next, symbol rotation and inversion is performed on only the first of M blocks for a total of $(2N/M)$ sequences in the first block. The combination with the smallest PAPR in the first block is stored. This process continues for each of the remaining $M-1$ blocks, resulting in a total of $2N$ inversions, as shown in Fig. 5.

3) Computational Complexity: In the optimal approach (O-CSRI), the number of possible sequences grows exponentially with N, assuming that the number of symbols in each block is constant. Thus, for large M, a significant number of comparisons is needed in order to locate the sequence with minimal PAPR. Complexity becomes prohibitively high and makes this approach impractical. However, the suboptimal algorithm (SS-CSRI) limits the total number of combinations to $2N$. Although the search space for the minimal PAPR is significantly reduced, the suboptimal algorithm still offers high performance [29]. Table I demonstrates the complexity reduction achieved by using the suboptimal approach when $N = 512$ subcarriers and $M = 16$ blocks are considered.

It should be mentioned that, despite the reduction of permutations performed by the suboptimal algorithm, the amount of

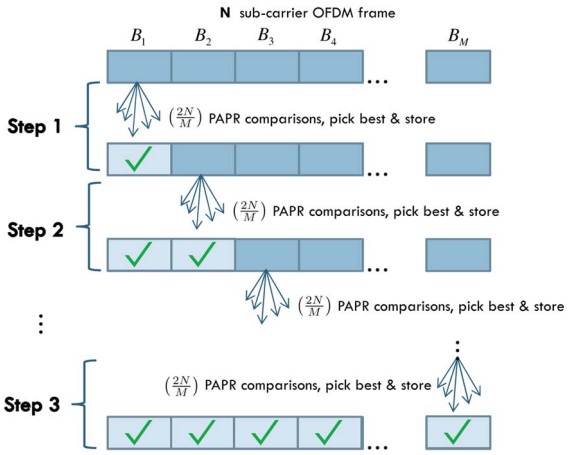

Fig. 5. Successive selection of minimal PAPR on a block-by-block basis in SS-CSRI algorithm.

TABLE I
COMPARISON OF ALGORITHM COMPLEXITY

Optimal (O-CSRI)	Sub-optimal (SS-CSRI)
$\underbrace{(\frac{2N}{M})\cdots(\frac{2N}{M})}_{M} = (\frac{2N}{M})^M$	$\underbrace{(\frac{2N}{M})+\cdots+(\frac{2N}{M})}_{M} = 2N$
$\approx 7.93x10^{28}$	1024

overhead necessary to decode the original OFDM sequence at the receiver is the same as that in the optimal approach, namely, $M\log_2(2N/M)$. The same amount of overhead is necessary in both approaches because the number of times that the symbols were rotated (as well as whether they were inverted or not) needs to be conveyed.

C. Novel PAPR-Reduction ABL Algorithm

To combine PAPR reduction and ABL techniques into a unified algorithm, modifications must be made to the SS-CSRI algorithm, as the original algorithm was not designed to work in the context of subcarrier-based modulation. A comparison of the modified algorithm and the original SS-CSRI algorithm is therefore provided in Fig. 6.

Unlike the conventional SS-SCRI algorithm, M is determined by the number of modulation orders selected by the ABL algorithm to transmit the OFDM sequence. For example, if the ABL algorithm determines that the optimal bit distribution uses a combination of BPSK, 4-QAM, and 16-QAM, the number of divisions, M, is 3. Dividing the OFDM sequence into the same number of blocks as modulation orders ensures that only data symbols of the same modulation order may be rotated and inverted. Since the blocks depend on channel conditions and vary in size, a check is performed to limit permutation when the number of blocks for a given modulation order is small. This avoids redundant permutation while still ensuring that the total number of permutations is maintained.

Assuming a range of M modulation orders and fixed number of permutations to be performed, N_p, the modified algorithm will first find the maximum permutations possible, K_{max}, for the modulation order allocated to the smallest number of subcarriers. The algorithm then finds K_{max} for the modulation order with the next smallest number of allocated subcarriers.

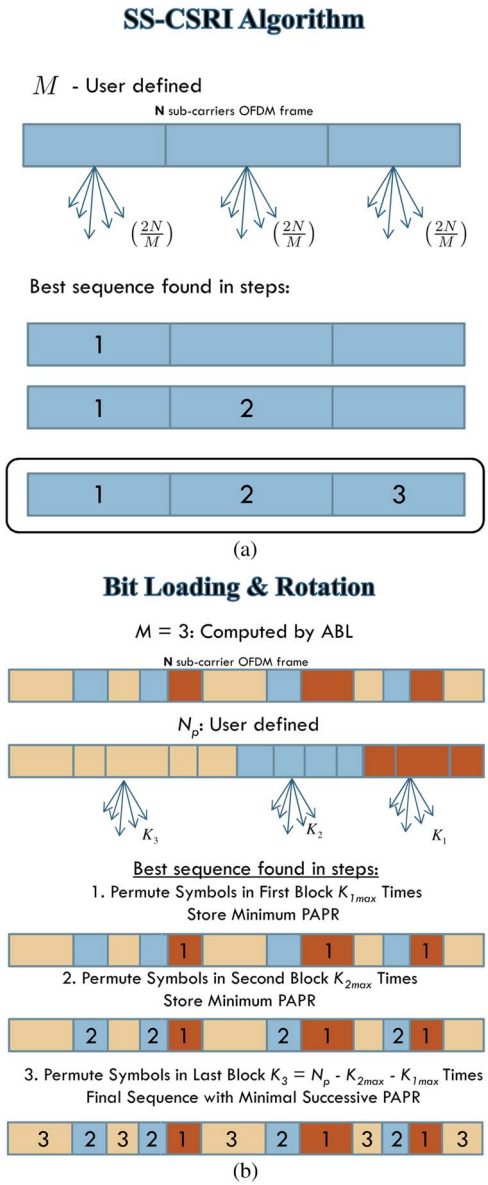

Fig. 6. Comparison of SS-CSRI and adaptive algorithms. (a) Minimal PAPR selection in SS-CSRI algorithm. (b) Minimal PAPR selection in adaptive algorithm.

This process continues for the remaining $M-2$ modulation orders. The final modulation order will then consist of $N_p - \sum_i^{M-1} K_{max_i}$ permutations such that the total number of permutations is the desired N_p.

To demonstrate the steps of the modified PAPR-reduction algorithm, a small example is provided. It is assumed in this example that $N_p = 90$ and three modulation orders, BPSK, 4-QAM, and 16-QAM, are used. Suppose the number of subcarriers allocated to each modulation rate is 41, 4, and 3, respectively [30]. Then, perform the following.

1) Find K_{max} for 16-QAM. With three subcarriers, a total of $3! = 6$ permutations is possible.
2) Find K_{max} for 4-QAM. With four subcarriers, a total of $4! = 24$ permutations is possible.
3) The remaining $90 - 6 - 24 = 60$ permutations are performed on subcarriers using BPSK-modulated data.

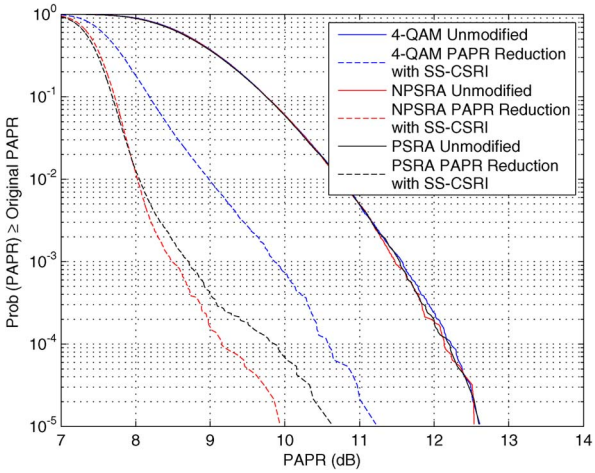

Fig. 7. Measured CCDF of PAPR for fixed-rate and adaptive physical layers.

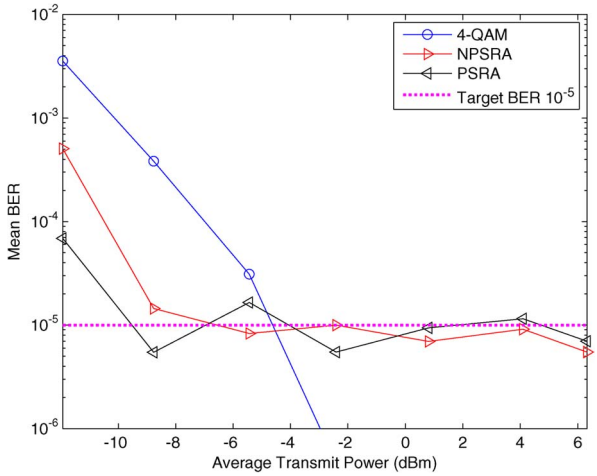

Fig. 8. Measured average BER versus average transmit power for fixed-rate and adaptive physical layers.

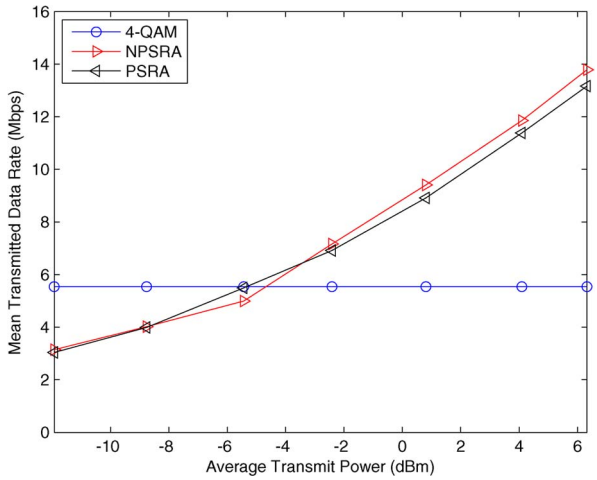

Fig. 9. Measured average transmitted data rate versus average transmit power for fixed-rate and adaptive physical layers.

For the adaptive algorithm implementation with fixed permutations, N_p, the amount of control overhead necessary is $M\log_2(N_p/M)$ bits, rather than the $M\log_2(2N/M)$ bits required in the original SS-CSRI implementation.

V. Measurements

A. Experimental Setup

Baseband signal processing is performed in MATLAB prior to loading the waveform into an Agilent N5182A MXG vector signal generator. The signal generator combines and up-converts baseband in-phase/quadrature signals for transmission over the ultrasonic channel using Panametrics A112-SRM transducers with 5-MHz bandwidth and 0.25-in nominal element size. The acoustic waveform passes through a 0.25-in-thick piece of mild steel designed to represent a typical naval bulkhead and is captured at passband with an Agilent 54833A Infiniium oscilloscope. Down-conversion of the signal to baseband and additional signal processing are performed in MATLAB. The transmit power presented in Figs. 8 and 9 was calculated from the root-mean-square driving voltage of the power amplifier and 50-Ω input impedance of the transducer. In the experimental setup, 512 carriers were used. The training sequence length was two OFDM symbols, and six pilot tones were spaced across the bandwidth in subcarriers 62, 125, 188, 324, 387, and 450.

B. Results

Measurements illustrated here demonstrate comparable performance of fixed-rate 4-QAM modulation and the proposed PAPR-reduction and ABL algorithm using both NPSRA and PSRA bit loading. First, three fixed-rate 4-QAM packets are transmitted consecutively to acquire an estimate of the EVM for each subcarrier. The NPSRA algorithm then calculates a suboptimal bit distribution according to the mean subcarrier-based EVM and transmitted three packets. The PSRA algorithm performs these same tasks. For each physical layer, a total of 9350 packets composed of ten OFDM data symbols were transmitted, and the complementary cumulative distribution function (CCDF) of the PAPR for $N_p = 120$ permutations was plotted (see Fig. 7). The mean BER (see Fig. 8) under a target BER constraint of 10^{-5} was also analyzed in addition to the mean transmitted data rates (see Fig. 9). A target BER of 10^{-5} was chosen for this proof of concept. However, the algorithm allows the user to specify the target BER. No forward error correction was applied in the aforementioned tests.

As noted by all three solid lines in Fig. 7, the PAPR of the original symbols prior to implementing the modified SS-CSRI algorithm are the same for fixed-rate 4-QAM and both forms of the adaptive algorithm. The SS-CSRI algorithm shows a 1.5-dB reduction in PAPR for fixed-rate 4-QAM. The PAPR reduction is enhanced by an additional 1.5 dB when applied to the ABL packets, resulting in an overall maximum 3 dB reduction in PAPR.

The mean BER under a target BER constraint of 10^{-5} can be seen in Fig. 8. Measured results show that the PAPR-reduced rate adaptive algorithm successfully adheres to the target BER of 10^{-5} over a large range of transmit powers. The fixed-rate 4-QAM modulation is not capable of achieving this. In fact, 4-QAM requires an approximate transmit power of roughly

−4 dBm to maintain the average BER constraint. The source of this increased error is the penalty of allocating bits equally to all subcarriers regardless of whether the channel can maintain the required signal integrity. Additionally, the error rate of fixed-rate 4-QAM drops well below the constraint at high transmit powers because no attempt is made to increase throughput, although channel conditions suggest that higher data rates are possible.

The use of fixed-rate OFDM alone increases data rates in the ultrasonic channel above the maximum 5 Mbps achievable using single-carrier techniques [18]–[24]. However, the use of the adaptive algorithm further increases the average transmitted data rate to roughly 14 Mbps at average transmit powers near 6 dBm. With respect to single-carrier communication techniques, the proposed algorithm achieves significant throughput improvements of roughly 280%. Measured results showing throughput with respect to average transmit power illustrate this improvement in Fig. 9, which clearly shows that the adaptive algorithm achieves larger average transmitted data rates than fixed 4-QAM modulation. Note that training overhead is not accounted for in these measurements. The slow-varying nature of the ultrasonic channel allows for minimal training and feedback of CSI, reducing overhead to a negligible factor when analyzing throughput.

Lastly, note that, although measured results are provided for a single bulkhead thickness of 0.25 in, the system can be implemented trivially to bulkheads of different thicknesses. Although the number of OFDM subcarriers may increase or decrease with bulkhead thickness, the underlying principles of the proposed algorithm would remain unchanged. The steps outlined in Section IV-C to combine ABL and PAPR reduction remain the same, as the number of subcarriers used in the algorithm is simply a variable that can be easily adjusted for various applications and wall thickness.

VI. Conclusion

Control network applications require data transfer through metallic structures without penetrating the metal obstruction. Ultrasonic through-metal communication is commonly used in such environments. However, current single-carrier communication techniques are limited in these ultrasonic through-metal channel applications due to acoustic echoing within the metallic barrier. OFDM can greatly improve data throughput in ultrasonic nonpenetrating through-metal communication links. Additional throughput improvement is achieved by increasing the spectral efficiency through subcarrier-based rate adaptive algorithms and exploiting the slow-varying nature of this particular channel that easily allows for the maintenance of the CSI required for rate adaptation. To address high PAPR and make more efficient use of transmission hardware, a symbol rotation and inversion PAPR-reduction algorithm is modified and implemented in the adaptive OFDM framework. Based on measured results, this adaptive algorithm is capable of increasing data rates by roughly 280% in comparison to conventional single-carrier techniques at average transmit powers of roughly 6 dBm. These results provide strong evidence that the bottleneck effect of employing ultrasound links in wireless networks can be mitigated to result in networks that can support higher data rate applications.

References

[1] D. Graham, J. Neasham, and B. Sharif, "Investigation of methods for data communication and power delivery through metals," *IEEE Trans. Ind. Electron.*, vol. 58, no. 10, pp. 4972–4980, Oct. 2011.

[2] V. Gungor and G. Hancke, "Industrial wireless sensor networks: Challenges, design principles, and technical approaches," *IEEE Trans. Ind. Electron.*, vol. 56, no. 10, pp. 4258–4265, Oct. 2009.

[3] K. Al Agha, M.-H. Bertin, T. Dang, A. Guitton, P. Minet, T. Val, and J.-B. Viollet, "Which wireless technology for industrial wireless sensor networks? The development of OCARI technology," *IEEE Trans. Ind. Electron.*, vol. 56, no. 10, pp. 4266–4278, Oct. 2009.

[4] Y. Ishii, "Exploiting backbone routing redundancy in industrial wireless systems," *IEEE Trans. Ind. Electron.*, vol. 56, no. 10, pp. 4288–4295, Oct. 2009.

[5] B. Lu and V. Gungor, "Online and remote motor energy monitoring and fault diagnostics using wireless sensor networks," *IEEE Trans. Ind. Electron.*, vol. 56, no. 11, pp. 4651–4659, Nov. 2009.

[6] J. Chen, X. Cao, P. Cheng, Y. Xiao, and Y. Sun, "Distributed collaborative control for industrial automation with wireless sensor and actuator networks," *IEEE Trans. Ind. Electron.*, vol. 57, no. 12, pp. 4219–4230, Dec. 2010.

[7] H. Sakuma, K. Nakamura, and S. Ueha, "Two-way communication over gas pipe-line using multicarrier modulated sound waves with cyclic frequency shifting," *Acoust. Sci. Technol.*, vol. 27, no. 4, pp. 225–232, 2006.

[8] P. Cheng, J. Chen, F. Zhang, Y. Sun, and X. Shen, "A distributed TDMA scheduling algorithm for target tracking in ultrasonic sensor networks," *IEEE Trans. Ind. Electron.*, vol. 60, no. 9, pp. 3836–3845, Sep. 2013.

[9] R. Luo and O. Chen, "Mobile sensor node deployment and asynchronous power management for wireless sensor networks," *IEEE Trans. Ind. Electron.*, vol. 59, no. 5, pp. 2377–2385, May 2012.

[10] Y. Hu, X. Zhang, J. Yang, and Q. Jiang, "Transmitting electric energy through a metal wall by acoustic waves using piezoelectric transducers," *IEEE Trans. Ultrason., Ferroelectr., Freq. Control*, vol. 50, no. 7, pp. 773–781, Jul. 2003.

[11] K. Wanuga, D. Dorsey, R. Primerano, and K. R. Dandekar, "Hybrid ultrasonic and wireless networks for naval control applications," in *Proc. ASNE Intell. Ships Symp. VII*, 2007.

[12] G. Saulnier, H. Scarton, A. Gavens, D. Shoudy, T. Murphy, M. Wetzel, S. Bard, S. Roa-Prada, and P. Das, "Through-wall communication of low-rate digital data using ultrasound," in *Proc. IEEE Ultrason. Symp.*, 2006, pp. 1385–1389.

[13] T. Hosman, M. Yeary, and J. Antonio, "Design and characterization of an MFSK-based transmitter/receiver for ultrasonic communication through metallic structures," *IEEE Trans. Instrum. Meas.*, vol. 60, no. 12, pp. 3767–3774, Dec. 2011.

[14] R. Primerano, "High Bit-Rate Digital Communication Through Metal Channels," Ph.D. dissertation, Drexel Univ., Philadelphia, PA, USA, Jul. 2010.

[15] R. Primerano, M. Kam, and K. Dandekar, "High bit rate ultrasonic communication through metal channels," in *Proc. 43rd Annu. CISS*, Mar. 2009, pp. 902–906.

[16] D. Graham, J. Neasham, and B. Sharif, "High bit rate communication through metallic structures using electromagnetic acoustic transducers," in *Proc. OCEANS Eur.*, May 2009, pp. 1–6.

[17] T. Murphy, "Ultrasonic digital communication system for a steel wall multipath channel: Methods and results," M.S. thesis, Rennselaer Polytechnic Institute, Troy, NY, USA, 2006.

[18] K. Wanuga, M. Bielinski, R. Primerano, M. Kam, and K. Dandekar, "High-data-rate ultrasonic through-metal communication," *IEEE Trans. Ultrason., Ferroelectr., Freq. Control*, vol. 59, no. 9, pp. 2051–2053, Sep. 2012.

[19] M. Bielinski, K. Wanuga, R. Primerano, M. Kam, and K. Dandekar, "Application of adaptive OFDM bit loading for high data rate through-metal communication," in *Proc. IEEE GLOBECOM*, Dec 2011, pp. 1–5.

[20] M. Bielinski, K. Wanuga, R. Primerano, M. Kam, and K. Dandekar, "High data rate adaptive ultrasonic OFDM physical layer for through-metal communications," in *Proc. ASNE Intell. Ships Symp. IX*, May 2011, pp. 1–8.

[21] M. Bielinski, K. Wanuga, R. Primerano, M. Kam, and K. Dandekar, "Transceiver design for high-data rate through-metal communication in naval applications," *Naval Eng. J.*, vol. 125, no. 1, pp. 121–126, Mar. 2013.

[22] T. Lawry, "A high performance system for wireless transmission of power and data through solid metal enclosures," Ph.D. dissertation, Rennselaer Polytechnic Inst., Troy, NY, USA, 2011.
[23] T. Lawry, K. Wilt, J. Ashdown, H. Scarton, and G. Saulnier, "A high-performance ultrasonic system for the simultaneous transmission of data and power through solid metal barriers," *IEEE Trans. Ultrason., Ferroelectr., Freq. Control*, vol. 60, no. 1, pp. 194–203, Jan. 2013.
[24] J. D. Ashdown, G. J. Saulnier, T. J. Lawry, K. R. Wilt, H. A. Scarton, S. Pascarelle, and J. D. Pinezich, "Multi-channel data communication through thick metallic barriers," in *Proc. IEEE ICC*, 2012, pp. 4678–4683.
[25] X. Li and L. J. Cimini, "Effects of clipping and filtering on the performance of OFDM," *IEEE Commun. Lett.*, vol. 2, no. 5, pp. 131–133, May 1998.
[26] V. Tarokh and H. Jafarkhani, "On the computation and reduction of the peak-to-average power ratio in multicarrier communications," *IEEE Trans. Commun.*, vol. 48, no. 1, pp. 37–44, Jan. 2000.
[27] P. Van Eetvelt, G. Wade, and M. Tomlinson, "Peak to average power reduction for OFDM schemes by selective scrambling," *Electron. Lett.*, vol. 32, no. 21, pp. 1963–1964, Oct. 1996.
[28] A. Jones, T. Wilkinson, and S. Barton, "Block coding scheme for reduction of peak to mean envelope power ratio of multicarrier transmission schemes," *Electron. Lett.*, vol. 30, no. 25, pp. 2098–2099, Dec. 1994.
[29] M. Tan and Y. Bar-Ness, "OFDM peak-to-average power ratio reduction by combined symbol rotation and inversion with limited complexity," in *Proc. IEEE GLOBECOM*, Dec. 2003, vol. 2, pp. 605–610.
[30] G. Sosa, "A joint bit loading and symbol rotation algorithm for multi carrier systems," M.S. thesis, Drexel Univ., Philadelphia, PA, USA, 2011.
[31] P. Chow, J. Cioffi, and J. Bingham, "A practical discrete multitone transceiver loading algorithm for data transmission over spectrally shaped channels," *IEEE Trans. Commun.*, vol. 43, no. 234, pp. 773–775, Feb.–Apr. 1995.
[32] D. Toumpakaris and J. Lee, "On the use of the gap approximation for the Gaussian broadcast channel," in *Proc. IEEE GLOBECOM*, Dec. 2010, pp. 1–5.
[33] J. Campello, "Optimal discrete bit loading for multicarrier modulation systems," in *Proc. IEEE Int. Symp. Inf. Theory*, Aug. 1998, p. 193.
[34] H. Ochiai and H. Imai, "On the distribution of the peak-to-average power ratio in OFDM signals," *IEEE Trans. Commun.*, vol. 49, no. 2, pp. 282–289, Feb. 2001.

Magdalena Bielinski (S'09) received the B.S. and M.S. degrees in electrical engineering from Drexel University, Philadelphia, PA, USA, in 2012, where she is currently working toward the Ph.D. degree.

Her research interests include link adaptation and multiple-input multiple-output channel modeling.

Guillermo Sosa (S'10–M'12) received the B.S. degree in electrical engineering from Universidad de la República in Montevideo, Montevide, Uruguay, in 2008 and the M.S. degree from Drexel University, Philadelphia, PA, USA, in 2011.

He is currently a Transmission Planning Engineer at "Telefónica Móviles Uruguay" and is also an IEEE collaborator in Uruguay.

Kevin Wanuga (S'07) received the B.S. and M.S. degrees in electrical and computer engineering from Drexel University, Philadelphia, PA, USA, where he is currently working toward the Ph.D. degree.

His research interests include spectrum sensing, cognitive and adaptive radio algorithms, and microwave techniques.

Richard Primerano (S'01–M'10) received the combined B.S. and M.S. degrees in electrical engineering and the Ph.D. degree from Drexel University, Philadelphia, PA, USA, in 2005 and 2010, respectively.

In 2010, he joined the Drexel University College of Engineering as an Assistant Professor. His professional interests include robotics, ultrasonic data communication, and radio-frequency communication system design. He is active in through-metal data communication research. His group investigates applications ranging from high data rate (tens of megabits per second) to very low cost/complexity.

Moshe Kam (S'75–M'77–SM'92–F'01) received the B.S. degree in electrical and electronics engineering from Tel Aviv University, Tel Aviv, Israel, in 1977 and the M.S. and Ph.D. degrees from Drexel University, Philadelphia, PA, USA, in 1985 and 1987, respectively.

He is currently the Department Head and Robert Quinn Professor of Electrical and Computer Engineering at Drexel University. He is also the Director of the Drexel University Data Fusion Laboratory. His research interests include detection and estimation, data fusion and team decision making, robotics and navigation, and engineering education.

Kapil R. Dandekar (S'95–M'01–SM'07) received the B.S. degree in electrical engineering from the University of Virginia, Charlottesville, VA, USA, in 1997 and the M.S. and Ph.D. degrees in electrical and computer engineering from the University of Texas at Austin, Austin, TX, USA, in 1998 and 2001, respectively.

He is currently an Associate Professor and Associate Dean for Research at Drexel University and the Director of the Drexel Wireless Systems Laboratory. His research interests involve multiple-input multiple-output ad hoc networks, reconfigurable antennas, free space optical communications, ultrasonic communications, and sensor networks.